PROPERTIES OF BALLOONING MODES IN THE PLANAR AXIS HELIOTRON CONFIGURATIONS WITH A LARGE SHAFRANOV SHIFT

N. NAKAJIMA,[a,b]* S. R. HUDSON,[c] and C. C. HEGNA[d]

[a]National Institute for Natural Sciences, National Institute for Fusion Science, 322-6 Oroshi, Toki 509-5292, Japan
[b]The Graduate University for Advanced Studies, Department of Fusion Science, (SOKENDAI), 322-6 Oroshi
  Toki 509-5292, Japan
[c]Princeton Plasma Physics Laboratory, P.O. Box 451, Princeton, New Jersey 08543
[d]University of Wisconsin-Madison, Department of Engineering Physics, Madison, Wisconsin 53706

In the three-dimensional magnetic confinement configurations, the results of local mode analyses of the ballooning modes in the covering space (quasi modes) cannot be directly connected by superposition to the global mode analyses of the ballooning modes in the configuration space (physical modes) because of the lack of symmetry. However, a qualitative relation has been established to connect the quasi modes to physical modes in planar axis heliotron configurations with a large Shafranov shift. This relation is based on the topological structure of the level surfaces of the eigenvalues of the quasi modes. High-beta magnetohydrodynamic equilibria in the inward-shifted Large Helical Device configuration are examined. It is shown that the core plasma stays in the second stability, and the peripheral plasma stays near the marginally stable state against ballooning modes.

I. INTRODUCTION

The stability of ballooning modes is significantly influenced by the local structure of the magnetic configuration, i.e., by the local magnetic shear and the local magnetic curvature. It is thus difficult to determine the general properties of ballooning modes in the three dimensional (3D) configurations. Also, in 3D configurations, there is a theoretical problem. There is no exact

*E-mail: nakajima@nifs.ac.jp

way to construct the physical modes in the configuration space from the superposition of the quasi modes in the covering space based on the high-mode-number ballooning equation.[1] In this paper, properties of the ballooning modes in both the covering space and the configuration space have been intensively investigated in planar axis heliotron configurations allowing a large Shafranov shift, like the Large Helical Device[2] (LHD). We show that the ballooning modes in the configuration space can be connected to the ballooning modes in the covering space through the topological structure of the level surfaces of the eigenvalues of the quasi modes in the (ψ, θ_k, α) space, where ψ, θ_k, and α are the label of the flux surfaces, the radial wave number, and the label of the magnetic field lines on a specified flux surface, respectively. Especially, recently established high-beta plasmas with $\beta \gtrsim 3\%$, where β is the ratio of the averaged kinetic pressure to the averaged magnetic pressure, are examined taking into account both the clarified ballooning properties and the experimental observations.[3]

The organization of the paper is as follows. The results of the local mode analyses in the covering space are shown in Sec. II, where the destabilization mechanism of the high-mode-number ballooning modes in the stellarator-like magnetic shear region and the relation of the ballooning modes in the covering space (quasi modes) to those in the configuration space (physical modes) are discussed. Since there is no exact way in 3D configurations to construct the physical modes from the superposition of the quasi modes, a conjecture on the physical modes is derived from the results of the quasi modes. Such a conjecture, which is based on the topological structure of the level surfaces of the eigenvalues of the quasi-modes in (ψ, θ_k, α) space, is proved in Sec. III by using the global mode analyses for Mercier stable and

unstable equilibria. Also, the relation between ballooning modes and interchange modes and the effects of the boundary condition imposed on the perturbations on the mode structure are examined. Section IV is devoted to analyzing the magnetohydrodynamic (MHD) stability of the high-beta MHD equilibria in inward-shifted LHD configurations on the basis of the properties of the ballooning modes. Using the local equilibrium variation method, we show that the core plasma stays in the second stability region, and the peripheral plasma stays near the marginally stable state against ballooning modes for equilibria similar to that observed experimentally. Summary and discussion are in Sec. V.

II. LOCAL MODE ANALYSES IN THE COVERING SPACE

The local mode analyses of the high-mode-number ballooning modes in the covering space are presented in this section. The destabilization mechanism of the high-mode-number ballooning modes in the stellarator-like magnetic shear region and the relation between quasi modes and physical modes is discussed. Although in the 3D configurations, the physical modes are not exactly constructed by the quasi modes, a conjecture on the physical ballooning modes is derived from the local mode analyses in the covering space.

II.A. Destabilization Mechanism

In the case of the planar axis heliotron configurations, like LHD consisting of two twisted helical coils with the same winding law with the toroidal field period M ($= 10$ for LHD) and three set of poloidal coils with up-down symmetry, the Shafranov shift is essentially axisymmetric and is fairly large due to the low vacuum rotational transform $\iota(\sim 0.4)$ near the magnetic axis. Since it is the Shafranov shift that makes the difference between the local magnetic shear, $\hat{s} = -\hat{s}_q$, and the global magnetic shear, $s = -s_q$, the difference between the local magnetic shear and the global magnetic shear $\hat{s} - s = -(\hat{s}_q - s_q)$ is essentially axisymmetric and large, where $\hat{s}$ (s) and $\hat{s}_q$ (s_q) are the local magnetic shear (global magnetic shear) in terms of ι and the safety factor $q = 1/\iota$, respectively. From these two essential characteristics of the Shafranov shift, a model equation of the local magnetic shear $\hat{s} = -\hat{s}_q$ is derived by using a stellarator expansion based on the high-beta ordering. The pressure in the whole plasma region must be treated in the high-beta ordering of tokamaks, namely, $\beta \sim O(\varepsilon_t)$, where $\varepsilon_t = a/R$ with the minor radius a and the major radius R so that the radial derivative of the Shafranov shift Δ becomes the order of unity: $d\Delta/dr \equiv \Delta' \sim O(1)$. The model equation of the local magnetic shear in standard tokamaks is usually derived by using low-beta ordering [where $\beta \sim O(\varepsilon_t^2)$ and so $\Delta' \sim O(\varepsilon_t)$] in the whole plasma region [except for a local region with a steep

pressure gradient, where $\beta \sim O(\varepsilon_t)$ and $\Delta' \sim O(1)$]. The model expression for $\hat{s}_q$ in tokamaks is derived in the region with a local steep pressure gradient. The model expression for the local magnetic shear $\hat{s}_q$ for the planar axis heliotron with large Shafranov shift and the standard tokamak is completely different[4]:

$$\hat{s}_q = s_q - \alpha \mathcal{F} \cos \eta \ ,$$

$$\mathcal{F} = \begin{cases} 1 \ , & \text{tokamaks} \\ \dfrac{1 + 3s_q + r\beta''/\beta'}{4} \ , & \text{LHD} \ , \end{cases} \quad (1)$$

where $s_q = (r/q)(dq/dr)$ and $\alpha = -R\beta'/\iota^2(> 0)$, and $' = d/dr$, respectively. The difference arises from whether the whole plasma region is treated in the high-beta ordering or not. In standard tokamaks with $s_q > 0$, the local magnetic shear $\hat{s}_q$ disappears for $\alpha \sim s_q$ in the outboard of the torus ($\eta = 0$), where the magnetic curvature due to toroidicity is locally unfavorable, and this leads to the destabilization of the high-n ballooning modes. In contrast, in planar axis heliotron configurations with a large Shafranov shift, the local magnetic shear $\hat{s}_q$ disappears in the outboard of the torus for $\alpha \sim 4s_q/(1 + 3s_q)$ near the radial position with the largest pressure gradient ($\beta'' = 0$), even in the stellarator-like magnetic shear region when the magnetic shear is fairly high ($s_q \lesssim -1$) (Ref. 4). This is the destabilizing mechanism of the high-mode-number ballooning modes in the stellarator-like magnetic shear region ($s_q < 0$) in the planar axis heliotron configurations with a large Shafranov shift like LHD. Note that a large Shafranov shift is needed to eliminate stabilizing effects by the local magnetic shear in the stellarator-like magnetic shear region. The 3D properties of the ballooning modes in the planar axis heliotron configurations are mainly due to the local magnetic curvature. Since the shape of the poloidal cross section of the LHD is a rotating ellipse, the local magnetic curvature consists of two parts. One is due to toroidicity, and the other is due to helicity. Even in the outboard of the torus, the magnetic curvature becomes locally favorable in the vertically elongated poloidal cross section, which manifests the 3D properties of the local magnetic curvature. In one toroidal turn, locally unfavorable and locally favorable magnetic curvatures alternatively appear in the outboard of the torus in the horizontally and vertically elongated poloidal cross sections, respectively. This strong magnetic field line dependence of the local magnetic curvature leads to the existence of 3D ballooning modes discussed in the following sections.

II.B. Relation Between Quasi Modes and Physical Modes

High-mode-number ballooning modes are analyzed in the covering space (ψ, η, α), where ψ, α, and η are the label of the flux surface or the toroidal flux, the label of the magnetic field line on a specified flux surface ψ, and

the coordinate along the magnetic field line specified by ψ and α, respectively. The covering space (ψ, η, α) is related to the straight field line magnetic coordinates (ψ, θ, ζ) as $\eta = \theta$ and $\alpha = \zeta - \theta/\iota$ (θ and ζ are poloidal and toroidal angles, respectively), and so two labels ψ and α are related to the magnetic field as $\vec{B} = \iota \nabla \alpha \times \nabla \psi$. By using flute-ordering with $|\vec{k}_\perp| \gg |k_\parallel|$, the incompressible quasi modes in the covering space are assumed to have an eikonal form: $\vec{\xi}_\perp = [(\vec{B} \times \vec{k}_\perp)/B^2] X e^{iS - i\omega t}$, where S is the eikonal and the perpendicular wave number $\vec{k}_\perp$ is expressed in terms of the eikonal as $\vec{k}_\perp \equiv \nabla S$, and so $S = S(\psi, \alpha)$. The slow change along a magnetic field line related to the parallel wave number $k_\parallel$ is expressed by the function X ($k_\parallel = \nabla_\parallel X/X$), which is governed by the incompressible ballooning equation. Consequently, the functions X and ω are the solution, or eigenfunction, and the frequency, or growth rate, of the high-mode-number incompressible ballooning equation. Since the high-mode-number ballooning equation is self-adjoint, the eigenvalue corresponding to the eigenfunction X is ω^2. The eigenfunction X and the eigenvalue ω^2 have the following parameter dependence in the three-dimensional magnetic configurations:

$$X = X(\eta | \psi, \theta_k, \alpha), \quad \omega^2 = \omega^2(\psi, \theta_k, \alpha) \ , \tag{2}$$

where θ_k is the radial wave number defined as $\theta_k = \partial_q S/\partial_\alpha S$, which comes from the perpendicular wave number $\vec{k}_\perp = \nabla S = \partial_\alpha S \nabla \alpha + \partial_q S \nabla q = \partial_\alpha S[\nabla \alpha + \theta_k \nabla q]$ (hereafter, the safety factor q is used instead of ψ). Note that the eigenfunction X and the eigenvalue ω^2 are independent of α in the axisymmetric tokamaks, because every magnetic field line in a specified flux surface is equivalent to the other in the covering space. The quasi modes in the covering space are not physical modes in the configuration space because they do not generally satisfy the double-periodic condition in both poloidal and toroidal directions. Thus, the relation of the quasi modes in the covering space to the physical modes in the configuration space must be established. The physical modes in the configuration space satisfying the double-periodic condition in both poloidal and toroidal directions are considered to be constructed by superposing the quasi modes with the same eigenvalue ω^2. This construction becomes possible when the eikonal satisfies the double periodic condition and single-valuedness with respect to q on a level surface of the eigenvalue $\omega^2(q, \theta_k, \alpha)$ (Ref. 1).

In axisymmetric tokamaks, the level surfaces of ω^2 in the 3D space (q, θ_k, α) become straight cylinders with the axis in the α direction because α is an ignorable coordinate, $\omega^2(q, \theta_k)$, so that those conditions are satisfied on a set of level surfaces of $\omega^2(q, \theta_k)$ or $\theta_k = \theta_k(q, \omega^2)$ for a set of eigenvalues ω^2. As a result, the semiclassical quantization condition is derived:

$$\frac{1}{2\pi} \oint dq \, \theta_k(q, \omega^2 = constant) = \frac{2N_r + 1}{2n} \ , \tag{3}$$

where n and N_r are the toroidal mode number and the radial node number, respectively (note that planar level surfaces of ω^2 infinitely continuous in the θ_k direction, which appear in fairly low magnetic shear region, are omitted here). The semiclassical quantization condition Eq. (3) means that the physical modes in the configuration space can be constructed from the quasi modes in the covering space when the eigenvalues ω^2 of the quasi modes satisfy the semiclassical quantization condition Eq. (3) for an adequately selected toroidal mode number n and radial node number N_r. In other words, the eigenvalue of physical modes ω^2_{phys} are distinguished by n and N_r: $\omega^2_{phys} = \omega^2_{phys}(n, N_r)$. This semiclassical quantization condition is also obtained by solving the ray equations on the level surfaces of eigenvalue $\omega^2(q, \theta_k)$ in the 3D space (q, θ_k, α) and by requiring the eikonal to be doubly periodic and single-valued in q (Ref. 1).

On the other hand, in 3D configurations, the eigenvalues of the quasi modes have α dependence, so the solution of the ray equations does not exactly satisfy the conditions that the eikonal be doubly periodic and single-valued in q. This leads to the result that physical modes in the configuration space are not exactly constructed from the quasi modes in the covering space. Thus, only a conjecture regarding such a construction is allowed. This fact reflects that the high-mode-number ballooning modes in the 3D configurations have such a strong toroidal mode coupling that the toroidal mode number n is not a good quantum number. To make a conjecture on the physical modes, the level surfaces of ω^2 in the (q, θ_k, α) space are calculated.[5] One example of the level surfaces of unstable normalized eigenvalues $\Omega^2 = \Omega^2(q, \theta_k = 0, \alpha)$ (≤ 0) in a Mercier-unstable equilibrium is shown in Fig. 1,
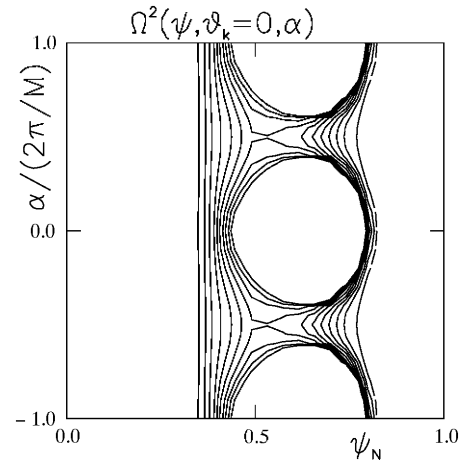

Fig. 1. The level surfaces of the normalized eigenvalues $\Omega^2(\psi, \theta_k = 0, \alpha)$ for Mercier-unstable MHD equilibrium in the standard LHD configuration. Note that ψ is used instead of q and that almost all parts of the level surfaces denoted by circles are omitted so that open circles are created.

where the currentless MHD equilibrium with the pressure profile $P(s) = P_0(1 - s^2)^2$ (s is the normalized toroidal flux) is used in the standard LHD configuration with the vacuum magnetic axis $R_{av} = 3.75$ m. The normalized eigenvalue is defined as $\Omega^2(q, \theta_k, \alpha) = \omega^2(q, \theta_k, \alpha)\tau_A^2(q)$, where $\tau_A(q)$ is the local poloidal Alfvén transit time defined as $\tau_A \equiv \sqrt{\rho_m/(2\pi\iota d\Phi_T/dV)}$ with the ion mass density ρ_m, the toroidal flux Φ_T, and the plasma volume V. The normalized eigenvalue Ω is used instead of ω to clearly show the topological structure. For the original eigenvalue ω, the topological structure is highly deformed through the ι dependence of τ_A. It is understood that two types of topological level surfaces exist, namely, lines and circles on the $(q(\psi), \alpha)$ plane with $\theta_k = 0$. From the results given by Fig. 1 and those in Ref. 5, the overall structure of the level surfaces of unstable eigenvalues $\omega^2(q, \theta_k, \alpha)$ (≤ 0) in the (q, θ_k, α) space is understood. The schematic pictures of the resultant level surfaces of the unstable eigenvalues ω^2 (≤ 0) in the planar axis heliotron configurations with a large Shafranov shift are shown in Fig. 2 together with the axisymmetric case. In Mercier-unstable equilibria, two types of topological level surfaces coexist in the Mercier-unstable region ($D_I > 0$) with stellarator-like global magnetic shear with $s = d \ln \iota/d \ln r (> 0)$. One type is cylindrical, like the tokamak case; the other is spherical. The latter resides inside the former. In Mercier-stable equilibria, only spherical level surfaces exist. The spherical level surfaces are separated along the α axis with a distance of $2\pi/M$, where M is the equilibrium toroidal field period, which comes from the fact that the ballooning-unstable magnetic field lines are localized in each toroidal field period (note that $\alpha = \zeta - \theta/\iota$). In the LHD case, as mentioned in Sec. II.A, such an unstable region corresponds to the horizontally elongated poloidal cross section. Note that, independent of the topology of the level surfaces, the magnitude of ω^2 increases (the quasi modes become more unstable) from outer level surfaces to inner level surfaces. From those results, the following conjecture on the physical finite-n ballooning modes is obtained[5]:

1. Spherical level surfaces correspond to 3D ballooning modes with strong toroidal mode coupling. Those modes will be destabilized for relatively high toroidal

mode numbers n, namely, $n > M$ or $n \gg M$ where M is the field periodicity.

2. Cylindrical level surfaces correspond to two-dimensional-like (2D-like) ballooning modes with weak toroidal mode coupling like those in tokamaks or interchange modes. Those modes will be destabilized for relatively low n, namely, $n \lesssim M$.

3. In Mercier-stable equilibria, only 3D ballooning modes with $n > M$ or $n \gg M$ might be destabilized.

4. In Mercier-unstable equilibria, both 3D ballooning modes with $n > M$ or $n \gg M$ and 2D-like ballooning modes or interchange modes with $n \lesssim M$ might be destabilized. The former should have larger growth rates than the latter.

5. In the cases of 2D-like ballooning modes and interchange modes, the toroidal mode number n might be a good quantum number so that the semiclassical quantization condition given by Eq. (3) might be applicable to them.

III. GLOBAL MODE ANALYSES IN THE CONFIGURATION SPACE

Global mode analyses have been performed for incompressible perturbations using the CAS3D code[6] to confirm the conjecture on finite-n ballooning modes in the configuration space. The properties of both ballooning modes and interchange modes and the relation of the ballooning modes to the interchange modes are clarified. Moreover, the effects of the boundary condition of the perturbations on the mode structure are discussed in this section.

III.A. In Mercier-Unstable Equilibria

Mercier-unstable equilibria[7] have recently been investigated in the LHD for both the inward-shifted LHD configuration with the vacuum magnetic axis at $R = 3.6$ m and in the standard LHD configuration with the vacuum magnetic axis at $R = 3.75$ m (Ref. 3). These equilibria are currentless with pressure profile $P(s) = P(0)(1 - s)$
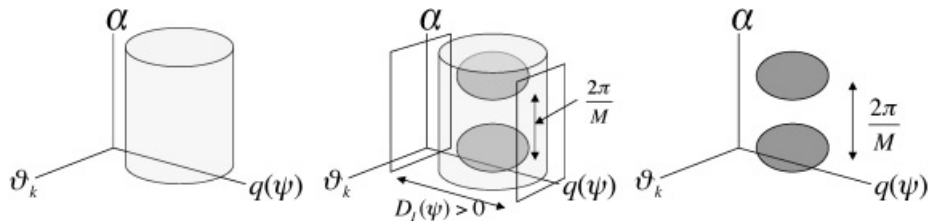

Fig. 2. The level surfaces of ω^2 for tokamaks (the first column), Mercier-unstable (the second column), and Mercier-stable (the third column) planar axis heliotron configurations with a large Shafranov shift.

$(1 - s^9)$ (s is the normalized toroidal flux). As is expected from the conjecture regarding the high-mode-number ballooning modes analyses, the toroidal mode coupling for modes with $n < M$ and with $n \sim M$ is indeed so weak that the toroidal mode number n is used as a good quantum number. Figures 3 and 4 show most unstable modes with $n = -4$ and with $n = -11$, respectively, for currentless MHD equilibria with $\beta_0 = 4\%$ (upper row) and with $\beta_0 = 8\%$ (lower row) in the inward-shifted LHD configuration, where β_0 indicates the β value at the magnetic axis. The differences between interchange modes and 2D-like ballooning modes are quite clear in the radial structure of the Fourier modes of the radial displacement $\xi \equiv \vec{\xi} \cdot \nabla s$ shown in the first columns of Figs. 3 and 4. In the case of the interchange modes, the radially adjacent Fourier modes have opposite signs; however, the radially adjacent Fourier modes have the same sign in 2D-like ballooning modes. This difference leads to the difference on the poloidal localization of the perturbed pressure. Although the differences between interchange modes and 2D-like ballooning modes are not so clear in the figures of the perturbed pressure profile, an interchange mode (a 2D-like ballooning mode) makes radially extended vortex-like structures on the inboard (outboard) of the torus. Such vortex-like structures of an interchange mode (a 2D-like ballooning mode) are radially split into many small vortex-like structures on the outboard (inboard) of the torus, which is discussed in Sec. III.C in detail. As is conjectured from the local mode analyses in the covering space, an interchange mode or a 2D-like ballooning mode is destabilized as the most unstable mode, depending on the β value, for low toroidal mode numbers with $n < M$ and moderate toroidal mode numbers with $n \sim M$. As β increases, the most unstable mode changes from an interchange mode into a 2D-like ballooning mode for low toroidal mode numbers with $n < M$ and moderate toroidal mode numbers with $n \sim M$. Note that which mode is destabilized as the most unstable mode between an interchange mode and a 2D-like ballooning mode depends strongly on the β values (in low-beta, ballooning modes are not destabilized) and weakly on the magnetic configurations.[7] Properties of ballooning modes and interchange modes and the relation between them are discussed in Sec. III.C in detail.
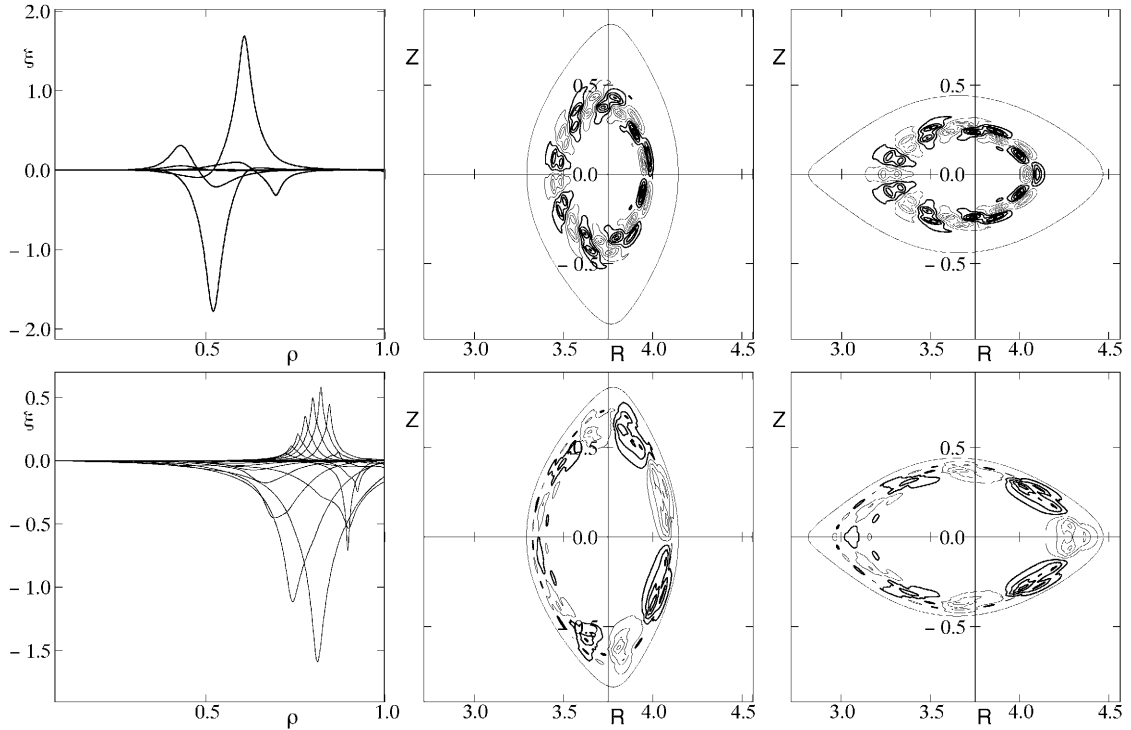

Fig. 3. Most unstable modes for $n = -4$ in the currentless MHD equilibria with $\beta_0 = 4\%$ (upper row) and with $\beta_0 = 8\%$ (lower row) in the inward-shifted LHD configuration. The figures in the first column indicate the radial profile of dominant Fourier modes of the radial displacement $\xi \equiv \vec{\xi} \cdot \nabla s$ as a function of the normalized minor radius $\rho = \sqrt{s}$, and the figures in the second and third columns denote contours of the perturbed pressure profile in the vertically and horizontally elongated poloidal cross sections of the Boozer coordinates, respectively, where incompressible perturbations are assumed under the free boundary condition. The 2D-like ballooning mode with $n = -4$ (lower row) has weak toroidal mode coupling so that a 2D-like ballooning mode with $n = -14$ is superposed. This superposition is most clearly seen in the first figure in the lower row.
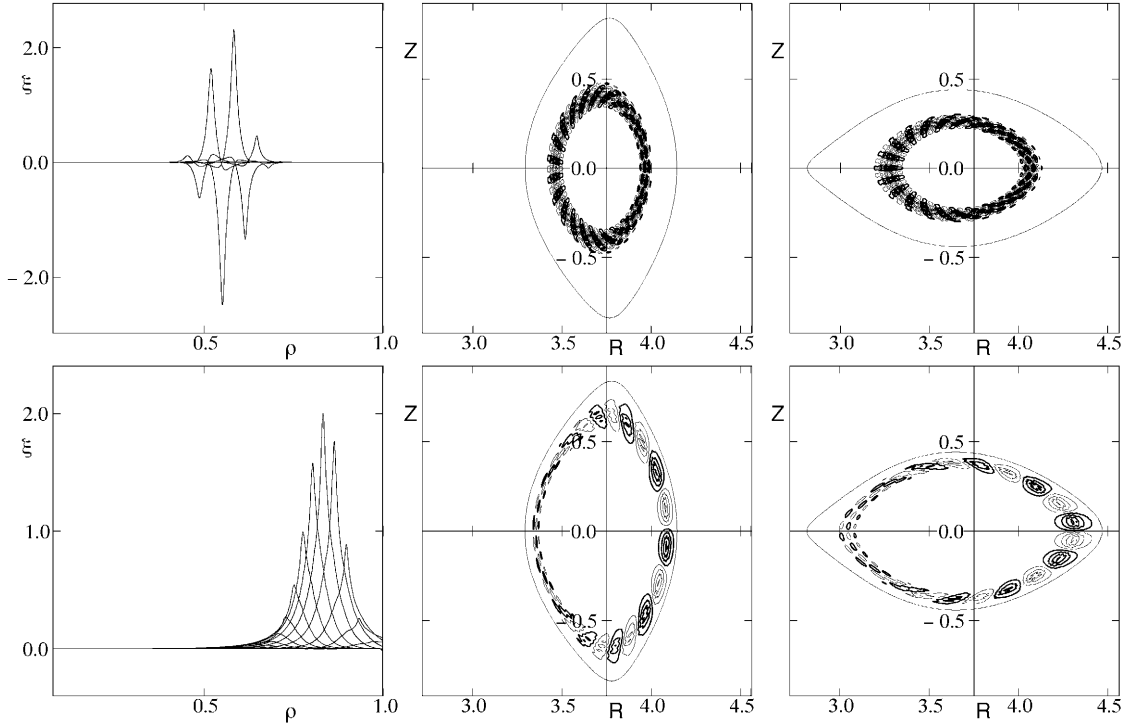
Fig. 4. Most unstable modes for $n = -11$ in the currentless MHD equilibria with $\beta_0 = 4\%$ (upper row) and with $\beta_0 = 8\%$ (lower row) in the inward-shifted LHD configuration. The figures in the first column indicate the radial profile of dominant Fourier modes of the radial displacement ξ as a function of $\rho = \sqrt{s}$, and the figures in the second and third columns denote contours of the perturbed pressure profile in the vertically and horizontally elongated poloidal cross sections of the Boozer coordinates, respectively, where incompressible perturbations are assumed under the free boundary condition.

For $n > M$ or $n \gg M$, 3D ballooning modes with strong toroidal mode coupling are destabilized as the most unstable modes, as is shown in Fig. 5 in the currentless MHD equilibria with $\beta_0 = 6\%$ in the standard LHD configuration with the vacuum magnetic axis at $R = 3.75$ m. As is understood from the radial profiles of the dominant Fourier modes, 3D ballooning modes consist of the superposition of the 2D-like ballooning modes with a single toroidal mode number n and multiple poloidal mode numbers. It is quite clear from the contours of the perturbed pressure in the poloidal cross sections that as the dominant toroidal mode number increases, the toroidal mode coupling becomes so significant that the 3D ballooning modes have a tendency to be localized in the flux tubes.

III.B. In Mercier-Stable Equilibria

The same types of global mode analyses have been performed for Mercier-stable equilibria in the standard LHD configuration (with the vacuum magnetic axis at $R = 3.75$ m). In Mercier-stable, currentless equilibria, low-beta plasmas are completely stable, and only 3D ballooning modes with strong toroidal mode coupling are destabilized as the most unstable modes at high beta,

as is shown in Fig. 6. As well as in the Mercier-unstable equilibria, the 3D ballooning modes consist of the superposition of the 2D-like ballooning modes with a single toroidal mode number n and multiple poloidal mode numbers, and the 3D ballooning modes have a tendency to be localized in the flux tubes as the toroidal mode numbers n increase.

From the aforementioned global mode analyses, it might be concluded that the conjecture from the local mode analyses is confirmed for both Mercier-unstable and Mercier-stable MHD equilibria. Note that many 3D ballooning modes with different growth rates and radial structures are excited for perturbations with $n > M$ and $n \gg M$ in both the high-beta Mercier-unstable and Mercier-stable MHD equilibria. Whether such 3D ballooning modes will be distinguished by their mode structures will be discussed in Sec. V.

III.C. Relation of Ballooning Modes to Interchange Modes

In the case of 2D-like ballooning modes, as is shown in Sec. III.A, the toroidal mode coupling is so weak that the toroidal mode number n is a good quantum number. Thus, the semiclassical quantization condition might be
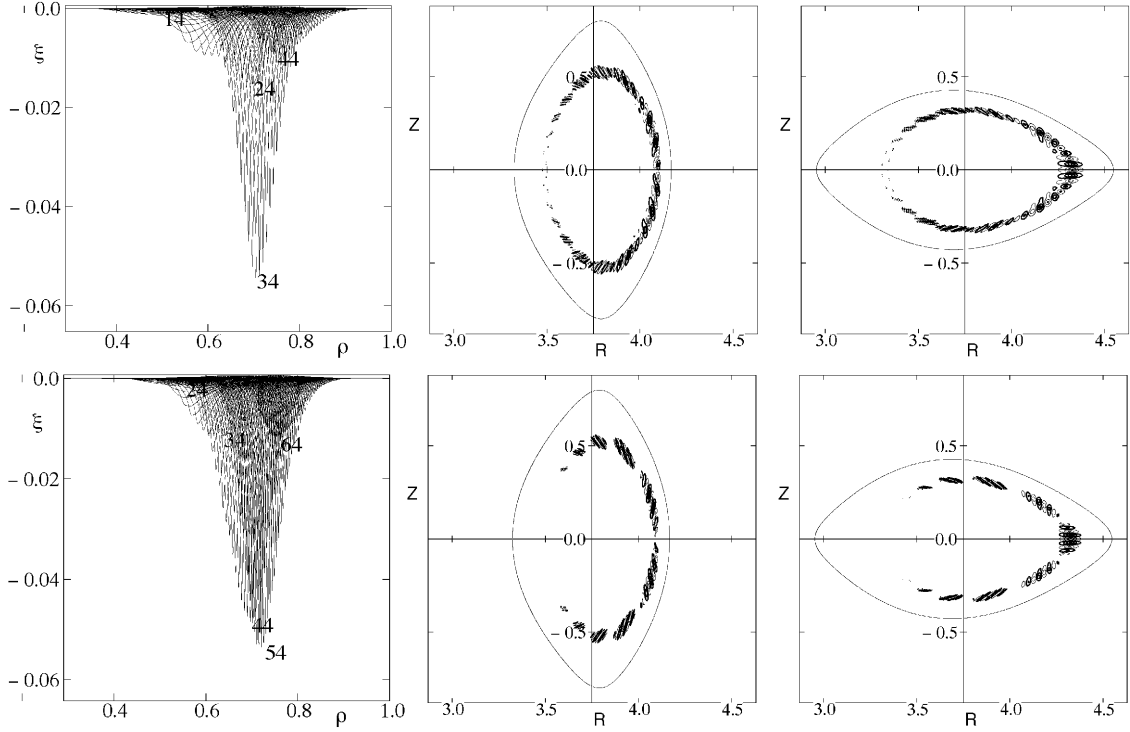
Fig. 5. Most unstable modes for $n > M$ (upper row) and $n \gg M$ (lower row) in the standard LHD configuration with the vacuum magnetic axis $R_{av} = 3.75$ m. The figures in the first column indicate the radial profile of dominant Fourier modes of the radial displacement ξ as a function of $\rho = \sqrt{s}$, and the figures in the second and third columns denote contours of the perturbed pressure profile in the vertically and horizontally elongated poloidal cross sections of the Boozer coordinates, respectively, where incompressible perturbations are assumed under the fixed boundary condition. The numbers in the figures in the first column denote the dominant toroidal mode numbers n.

approximately applicable. In other words, the eigenvalues ω^2 will be distinguished by both the toroidal mode number n and the radial node number N_r; $\omega^2 = \omega^2(n, N_r)$. This expectation is qualitatively confirmed, as is shown in Fig. 7, for the Mercier-unstable, currentless equilibrium with $\beta_0 = 8\%$ used in Figs. 3 and 4. The eigenvalues of the 2D-like ballooning modes with the same dominant toroidal mode number n are distinguished by the radial node number N_r. For the same radial node number N_r, the growth rates of 2D-like ballooning modes increase with the toroidal mode number n. As the radial node number N_r increases, the growth rates of the 2D-like ballooning modes with the same toroidal mode number n become smaller. Both dependences are consistent with the semiclassical quantum condition given by Eq. (3).

Those properties of 2D-like ballooning modes given by the semiclassical quantization condition are also seen for the interchange modes. Indeed, such properties are proved by comparing the eigenvalues obtained by global mode analyses to those by local mode analyses.[8] Here, a qualitative but more instructive and intuitive method will be used. The radial structures of the Fourier modes of the radial displacement $\xi \equiv \vec{\xi} \cdot \nabla s$ of the interchange modes are absolutely different from those of the 2D-like bal-

looning modes, as is understood from the figures in the first column of Figs. 3 and 4. However, by shifting the origin of the poloidal angle from the outboard side to inboard side of the torus, the properties of the radial localization of the interchange modes become clear.[7] Usually, the origin of the poloidal angle is on the outboard of the torus in a global Fourier code such as CAS3D. In the magnetic coordinate system (ψ, θ, ζ) used in CAS3D, the radial displacement ξ is Fourier decomposed as

$$\xi(\psi, \theta, \zeta) = \sum_{m,n} \xi_{m,n}(\psi) \cos[m\theta + n\zeta] \ . \qquad (4)$$

On the outboard of the torus with $\theta = 0$ on the poloidal cross section with $\zeta = 0$, Eq. (4) becomes

$$\xi(\psi, 0, 0) = \sum_{m,n} \xi_{m,n}(\psi) \ , \qquad (5)$$

and on the inboard of the torus with $\theta = \pi$ on the poloidal cross section with $\zeta = 0$, Eq. (4) becomes

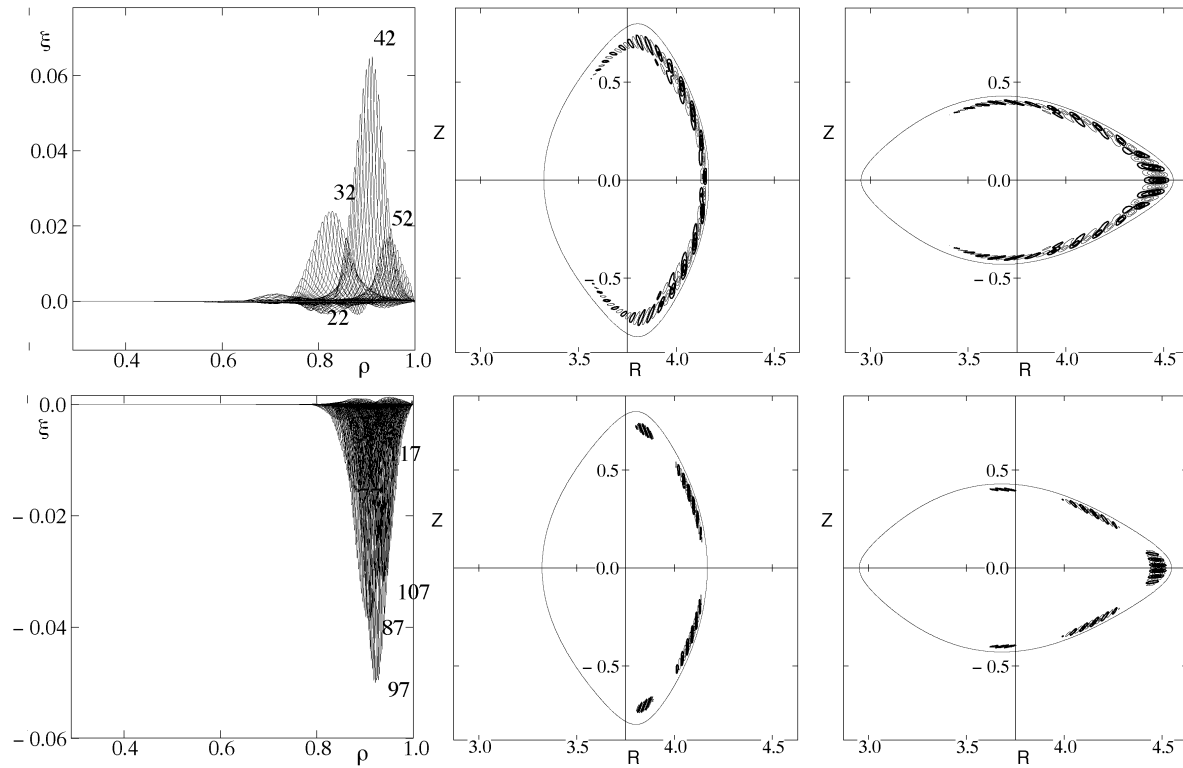$$\xi(\psi, \pi, 0) = \sum_{m,n} \xi_{m,n}(\psi)(-1)^m \ . \qquad (6)$$

Fig. 6. Most unstable modes for $n > M$ (upper row) and $n \gg M$ (lower row) in the currentless Mercier-stable MHD equilibria with $\beta_0 = 8\%$ in the standard LHD configuration, where the pressure profile is $P(s) = P(0)(1 - s)^2$. The figures in the first column indicate the radial profile of dominant Fourier modes of the radial displacement ξ as a function of $\rho = \sqrt{s}$, and the figures in the second and third columns denote contours of the perturbed pressure profile in the vertically and horizontally elongated poloidal cross sections of the Boozer coordinates, respectively, where incompressible perturbations are assumed under the fixed boundary condition. The numbers in the figures in the first column denote the dominant toroidal mode numbers n.
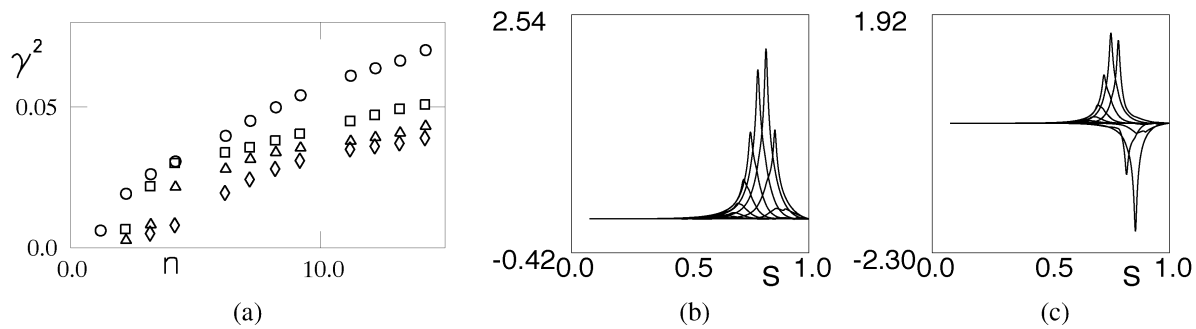

Fig. 7. (a) The square of the growth rates $\gamma^2 = -\omega^2$ in terms of the toroidal mode number n, where the eigenvalues are distinguished by the radial node number N_r for each toroidal mode number n. The circles, rectangles, triangles, and diamonds correspond to $N_r = 0$, 1, 2, and 3, respectively. The unstable modes with $n \geq 6$ ($n \leq 4$) correspond to 2D-like ballooning (interchange) modes. As the examples, the radial profiles of the dominant Fourier modes of the radial displace-ment ξ with $n = 9$ are shown as the function of the normalized toroidal flux s for (b) the most unstable ballooning mode with $N_r = 0$ and for (c) the second most unstable ballooning mode with $N_r = 1$. The square of the growth rate γ^2 corresponding to the ballooning modes with $N_r = 0$ ($N_r = 1$) is indicated by the circle (rectangle) for $n = 9$ in (a). Here, the Mercier-unstable MHD equilibrium with $\beta_0 = 8\%$ in Figs. 3 and 4 is used. In those analyses, incompressible pertur-bations are used under the fixed boundary condition.
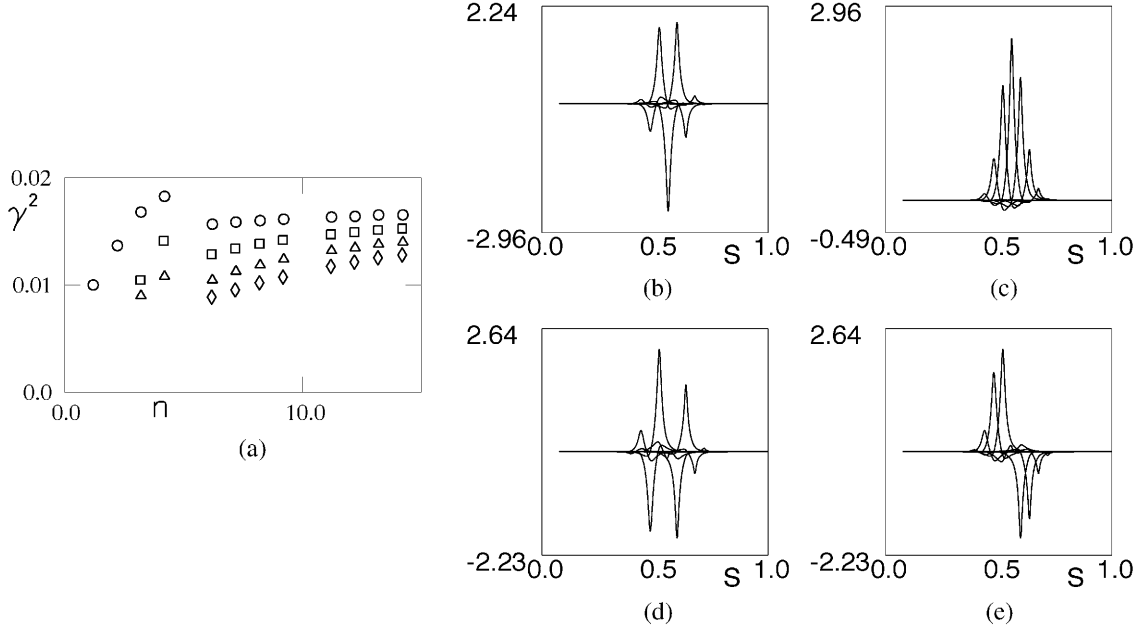
Fig. 8. (a) The square of the growth rates $\gamma^2 = -\omega^2$ in terms of the toroidal mode number n, where the eigenvalues are distinguished by the radial node number N_r for each toroidal mode number n. The circles, rectangles, triangles, and diamonds correspond to $N_r = 0$, 1, 2, and 3, respectively. The radial profiles of the dominant Fourier modes of ξ with $n = 9$ (b) for the most unstable interchange mode with $N_r = 0$ are shown as the functions of the normalized toroidal flux s for the original form and (c) for the form with the shift of the poloidal angle from outboard to inboard of the torus. The same quantities for the second most unstable interchange mode with $N_r = 1$ are shown (d) for the original form and (e) for the form with the shift of the poloidal angle from outboard to inboard of the torus. The square of the growth rate γ^2 corresponding to the interchange modes with $N_r = 0$ ($N_r = 1$) is indicated by the circle (rectangle) for $n = 9$ in (a). Here, Mercier-unstable MHD equilibrium with $\beta_0 = 4\%$ in Figs. 3 and 4 and incompressible perturbations under the fixed boundary condition are used.

Thus, when ξ corresponds to a 2D-ballooning mode, $\xi_{m,n}(\psi)$ has the same sign independently of the poloidal mode numbers, as is shown in the lower figure in the first column of Figs. 3 and 4 and in Fig. 7b. The eigenfunction localizes on the outboard of the torus, as is understood by Eq. (5). When ξ corresponds to an interchange mode, $\xi_{m,n}(\psi)$ has the opposite sign between adjacent poloidal modes: Fourier modes with even poloidal mode numbers have the opposite sign to Fourier modes with odd poloidal mode numbers, as is shown in the upper figure in the first column of Figs. 3 and 4 and in Figs. 8b and 8d. The eigenfunction now localizes on the inboard of the torus, as is understood by Eq. (6). The shift of the origin of the poloidal angle from outboard to inboard of the torus corresponds to replacing θ in Eq. (4) by $\theta - \pi$ so that

$$\xi(\psi,\theta,\zeta) = \sum_{m,n} \xi_{m,n}(\psi)(-1)^m \cos[m\theta + n\zeta] \ . \quad (7)$$

Thus, on the inboard of the torus with $\theta = 0$ and $\zeta = 0$, Eq. (7) becomes

$$\xi(\psi,0,0) = \sum_{m,n} \xi_{m,n}(\psi)(-1)^m \ , \quad (8)$$

which means that the interchange modes localize on the inboard of the torus. Thus, in the cases of 2D-like ballooning modes (interchange modes), the Fourier modes of the radial displacement ξ are in phase outboard (inboard) of the torus. From this difference on the poloidal localization, an interchange mode (a 2D-like ballooning mode) makes radially extended vortex-like structures inboard (outboard) of the torus. Such vortex-like structures of an interchange mode (a 2D-like ballooning mode) are radially split into many small vortex-like structures outboard (inboard) of the torus. Moreover, by using this difference, the radial node number of the interchange modes is distinguished as well as for the ballooning modes. In the case of the ballooning modes localizing outboard of the torus, the radial node number can be counted on the outboard of the torus, as is done in Fig. 7. In the case of the interchange modes localizing inboard of the torus, the radial node number can be counted in the inboard of the torus. By using those properties, the interchange modes with the same toroidal mode number n are also distinguished by the radial node number N_r. The examples are shown in Fig. 8, where the Mercier-unstable, currentless equilibrium with $\beta_0 = 4\%$ is again used, as in Figs. 3 and 4. In Fig. 8, all the modes are interchange

modes, and the properties expected from the semiclassical quantization condition, given by Eq. (3), are clearly seen for the modes with $n \geq 6$. For the modes with $n \leq 4$, the monotony of the growth rate with respect to n is lost, because the Fourier components of such low-n modes have such a wide radial structure that their properties are not completely determined by the local structure around their rational surfaces. It is quite clear that both 2D-like ballooning modes and interchange modes are distinguished by both the toroidal mode number n and the radial node number N_r, which means that the semiclassical quantization condition is applicable to both modes.

III.D. Effects of the Boundary Condition of the Perturbation

The effects of the boundary condition of the perturbations on the mode structure are considered in the Mercier-unstable MHD equilibria in the inward-shifted LHD configuration. Under the fixed boundary condition with $\xi(a) = 0$, each Fourier mode does not expand so much in the radial direction, and the radial overlapping of the Fourier modes is restricted. However, under the free boundary condition with $\xi(a) \neq 0$, the radial overlapping is allowed to some extent, which leads to the change in the mode structure from an interchange mode to a 2D-like ballooning mode, when the MHD equilibrium is slightly unstable or near the marginally stable state against ballooning modes. The ballooning modes induced by the free boundary condition are named freeboundary-induced ballooning modes. Such an example is shown in Fig. 9. Under the fixed boundary condition, the eigenfunction with $n = 2$ shows interchange structure (Fig. 9b), which changes into a 2D-like ballooning structure under the free boundary condition (Fig. 9c). The effects of the free boundary condition are significant for low-n modes because the radial extension of each Fourier mode becomes wider for lower toroidal mode number n, which is reflected in the significant differences of

the growth rates of the low-n perturbations between fixed and free boundary conditions as is shown in Fig. 9a. Thus, it is important to use the free boundary condition for perturbations in the global mode analyses, partially because the growth rate under the free boundary condition is larger than that under the fixed boundary condition, and partially because effects of the radially global perturbations under the free boundary condition on MHD equilibrium become more significant than those by the radially localized perturbations under the fixed boundary condition.

As is shown in Fig. 9a, the enhanced destabilization effect of the free boundary condition becomes weaker as the toroidal mode number n increases for the MHD equilibria with sufficiently small pressure gradient near the plasma boundary. However, when the pressure gradient is steep near the plasma boundary, the eigenfunction of ballooning modes or interchange modes extends up to the plasma boundary. In such cases, the calculation of modes with a high toroidal mode number ($n > M$) must be done under the free boundary condition. Note that the free-boundary-induced ballooning modes are the pressure-driven modes, so that they are different from the peeling modes, which are essentially current-driven modes, in tokamaks.

IV. MHD STABILITY ANALYSES OF HIGH-BETA EQUILIBRIA IN THE INWARD-SHIFTED LHD CONFIGURATIONS

Based on the properties of the ballooning modes and interchange modes clarified by the local and global mode analyses, MHD stability analyses of high-beta equilibria in the inward-shifted LHD configurations are performed.[9] The changes of the equilibrium quantities with β are shown in Fig. 10, where the currentless free boundary equilibria with pressure profile $P(s) = P(0)(1 - s)$
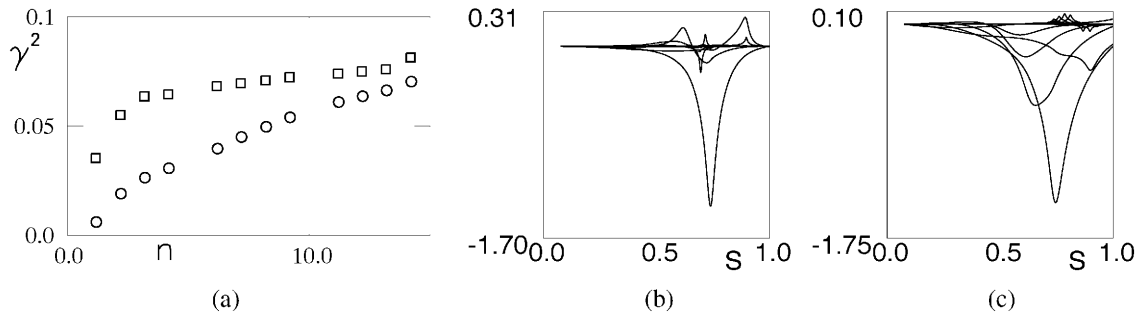

Fig. 9. (a) The square of the growth rates γ^2 of the most unstable modes in terms of the toroidal mode number n for fixed boundary $\xi(a) = 0$ (circles) and for the free boundary condition $\xi(a) \neq 0$ (rectangles). The radial profiles of the dominant Fourier modes of ξ with $n = 2$ for the most unstable mode are shown as functions of the normalized toroidal flux (b) under the fixed boundary condition and (c) under the free boundary condition. Here, Mercier-unstable MHD equilibrium with $\beta_0 = 8\%$ in Figs. 3 and 4 is used.
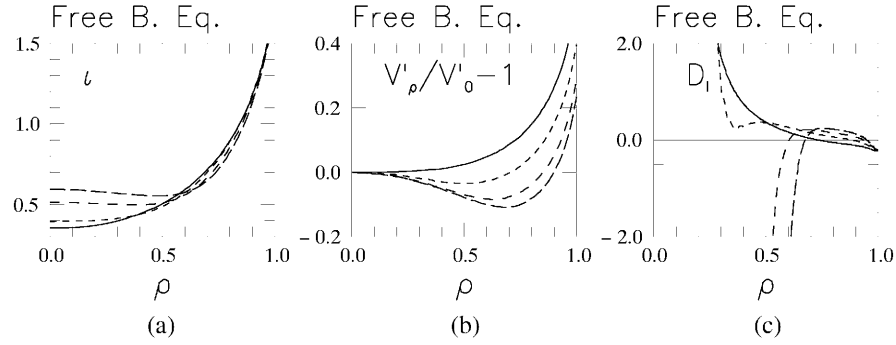
Fig. 10. (a) The change in the radial profile of the rotational transform ι, (b), in the magnetic well, and (c) in the Mercier criterion with β. The solid, short-dashed, middle-dashed, and long-dashed lines correspond to $\beta = 1, 2, 3,$ and 4%, respectively.

$(1 - s^9)$ are used. The conditions for the MHD equilibria, namely the free boundary condition, the currentless condition, and the chosen pressure profile, reflect the experimental observations. The key points are that the Mercier criterion is significantly improved by the magnetic well formation and that the dangerous $\iota = \frac{1}{2}$ rational surface disappears as β increases. Those improvements are brought by the Shafranov shift of the whole plasma. The corresponding normalized growth rates $\gamma \tau_{A0}$ of the most unstable modes, where τ_{A0} is the poloidal Alfvén transit time at the magnetic axis, are shown in Fig. 11 as functions of β under the various perturbation conditions. In any case, strong stabilization (self-stabilization) is seen as β increases. The growth rates of the most realistic perturbations, namely, compressible perturbations under

the free boundary condition $\xi(a) \neq 0$, are in the range of the ion diamagnetic frequency, so those modes are considered to be harmless. An important point is that the free-boundary-induced ballooning modes are destabilized at high-beta. To examine this situation in detail, the method of the equilibrium profile variations[10,11] has been applied to the MHD equilibria. This method of equilibrium profile variation is a very powerful means of investigating the stability margin of the equilibrium against high-mode-number ballooning modes and yields the $d\iota/d\psi - dP/d\psi$ stability diagram corresponding to the $s - \alpha$ diagram in tokamaks. Figure 12 shows typical examples.

Judging from the direction of the shift of MHD equilibrium according to β value and the position of MHD
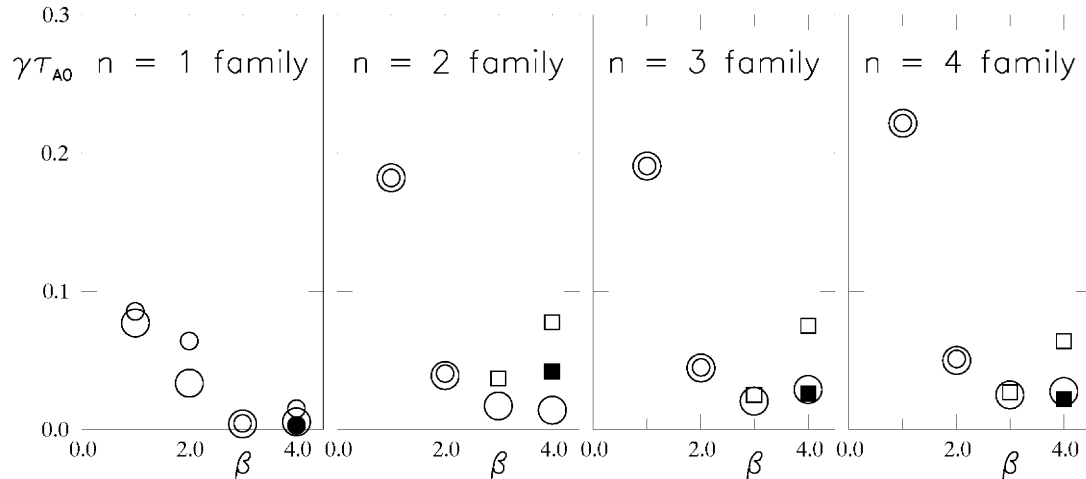

Fig. 11. The normalized growth rates $\gamma \tau_{A0}$ of the most unstable modes versus β for various perturbation conditions for four mode families. The large open circles (with small open circles and small open rectangles) correspond to incompressible perturbations under the fixed (free) boundary condition. The large open circles and small open circles (small open rectangles) indicate interchange modes (free-boundary-induced ballooning modes). The small solid rectangles and a small solid circle at $\beta = 4\%$ correspond to compressible perturbations under the free boundary condition and the small solid rectangles (a small solid circle) indicate free-boundary-induced ballooning modes (an interchange mode).
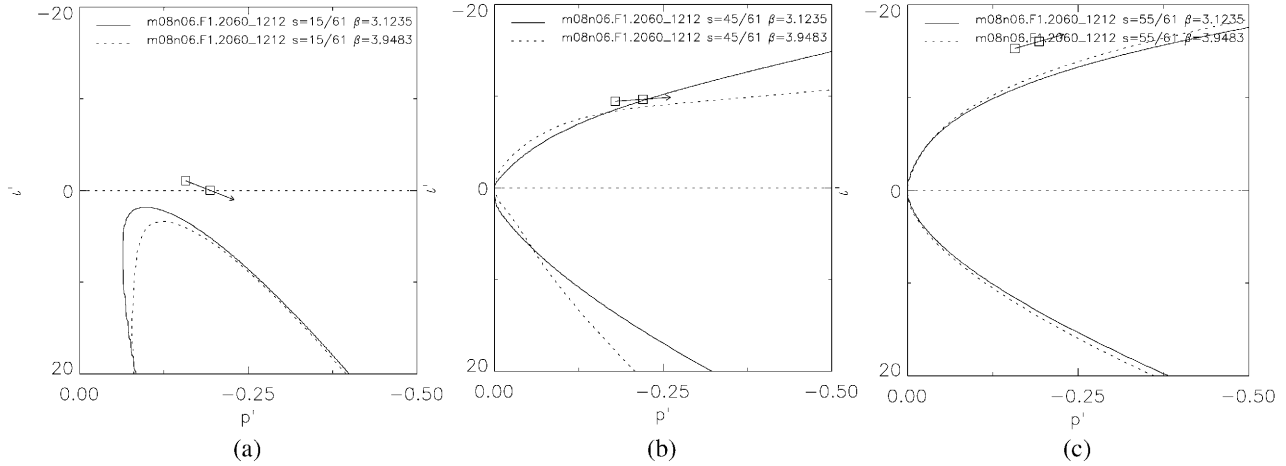
Fig. 12. The $d\iota/d\psi - dP/d\psi$ stability diagram (a) in the plasma core, (b) in the plasma periphery, and (c) in the plasma edge. The horizontal and vertical axes correspond to $-s_q$ and α in the $s_q - \alpha$ diagram of tokamak plasmas. The solid (dashed) curves indicate the stability boundary of high-mode-number ballooning modes for $\beta = 3\%$ ($\beta = 4\%$). Two squares attached to the arrow in each graph indicate the positions of (ι', P') corresponding MHD equilibria at $\beta = 3\%$ and $\beta = 4\%$. The arrows denote the direction of the shift of (ι', P') corresponding to the MHD equilibrium as β increase from $\beta = 3\%$ to $\beta = 4\%$. The MHD equilibria are the same as those in Figs. 10 and 11.

equilibria relative to the stability boundary, it might be concluded that the core region stays in the second stability state, the peripheral region stays near the marginally stable state, and the edge region stays in the first stability state. In the MHD equilibria used here, the pressure gradient near the plasma edge is quite small compared to the plasma periphery, so the Mercier criterion changes from Mercier unstable in the plasma periphery to Mercier stable near the plasma edge. This fact leads to the quantitative difference of the aforementioned ballooning stability between the plasma periphery and the plasma edge. When the equilibria have a finite pressure gradient at the plasma boundary, the difference between the plasma periphery and the plasma edge becomes ambiguous.

V. SUMMARY AND DISCUSSIONS

The research on the ballooning modes in the planar axis heliotron configurations allowing a large Shafranov shift like the LHD are summarized systematically, with particular attention given to the high-beta MHD equilibria in the inward-shifted LHD configurations. The relation of the quasi modes to physical modes, the relation between ballooning modes and interchange modes, and also the effects of the boundary condition of the perturbations on the pressure-driven modes are clarified.

In the 3D magnetic confinement configurations, the results of local mode analyses of the ballooning modes (quasi modes) in the covering space along the magnetic field line cannot be directly connected to those of the global mode analyses of the ballooning modes in configuration space (physical modes), because the rule

of superposition of the quasi modes is not allowed because of the lack of symmetry. In other words, the eikonal $S(\psi, \alpha)$, where ψ and α are the label of the flux surfaces and magnetic field lines, respectively, cannot be determined, so the phase relation of the quasi modes with the same eigenvalue is not established in superposing the quasi modes. However, in planar axis heliotron configurations with a large Shafranov shift, a qualitative relation has been established that the quasi-ballooning modes in the covering space can be connected to physical ballooning modes in the configuration space. Such a relation comes from the topological structure of the level surfaces of the eigenvalues in the (ψ, θ_k, α) space, where ψ, θ_k, and α are the label of the flux surfaces, the radial wave number, and the label of the magnetic field line on a flux surface, respectively. In the 3D magnetic configurations, two types of level surfaces exist in the (ψ, θ_k, α) space. One is the topologically spheroidal level surfaces, and the other is topologically cylindrical level surfaces. The former's quasi modes correspond to the 3D ballooning modes inherent to 3D configurations consisting of both relatively high poloidal and toroidal mode numbers through strong poloidal and toroidal mode coupling. The latter's quasi modes correspond to the 2D ballooning modes with fairly weak toroidal mode couplings, which are similar to those in the axisymmetric configurations, and to interchange modes. In the Mercier stable MHD equilibria, only 3D ballooning modes inherent to 3D configurations might be excited. In the Mercier unstable MHD equilibria, not only 3D ballooning modes as well as in the Mercier stable equilibria but also 2D ballooning modes and/or interchange modes might be excited. Since the latter has the topologically cylindrical level surfaces of
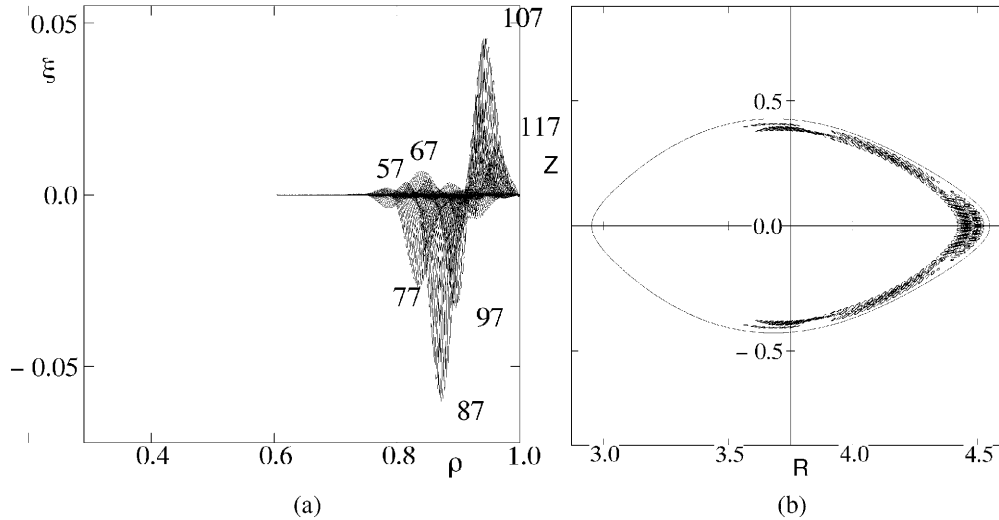
Fig. 13. The 3D ballooning modes in the same MHD equilibrium as that in Fig. 6: (a) the radial profile of dominant Fourier modes as a function of $\rho = \sqrt{s}$ with the dominant toroidal mode numbers and (b) contours of the perturbed pressure profile in the horizontally elongated poloidal cross section, where incompressible perturbations are assumed under the fixed boundary condition.

eigenvalues of quasi modes in the (ψ, θ_k, α) space, the approximate quantization condition connecting the quasi modes in the covering space to physical modes in the configuration space is applicable to them. Note that the quantization condition can be applicable to both 2D ballooning modes and interchange modes. Two-dimensional ballooning modes and interchange modes have smaller growth rates than those of 3D ballooning modes. Based on understanding of the properties of the ballooning modes and by using the equilibrium profile variation method, it is shown that recently achieved high-beta MHD equilibria in the inward-shifted LHD configurations stay in the second stable state in the plasma core and near the marginally stable state in the plasma periphery.

Since the high-beta plasmas in the inward-shifted LHD configurations stay near the marginally stable state in the plasma peripheral region, it should be clarified whether the experimentally suggested pressure profiles result from the ballooning instabilities or not.

Another interesting point is whether 3D ballooning modes are systematically distinguished or not. Figure 13 shows an example of the 3D ballooning modes, where the same Mercier-stable MHD equilibrium as that in Fig. 6 is used. The typical structure of this 3D ballooning mode is that it has one radial node ($N_r = 1$) at the averaged minor radius $\rho = \sqrt{s} \sim 0.92$. As is mentioned in relation to Figs. 5 and 6, 3D ballooning modes consist of the superposition of the 2D-like ballooning modes. Thus, if there is a rule in the superposition, then 3D ballooning modes might be systematically distinguished by the radial node numbers N_r and the behavior of the poloidal localization, for example, the number of the poloidal nodes created by the localization in the flux tubes. This point is associated with the integrability condition of the two-degrees-of-freedom Hamiltonian system related to the ray equations of the eikonal. These two points will be investigated in the near future.

REFERENCES

1. R. L. DEWAR and A. H. GLASSER, *Phys. Fluids*, **26**, 3038 (1983).

2. A. IIYOSHI et al., *Nucl. Fusion*, **39**, 1245 (1999).

3. O. MOTOJIMA et al., *Nucl. Fusion*, **43**, 1674 (2003).

4. N. NAKAJIMA, *Phys. Plasmas*, **3**, 4545 (1996).

5. N. NAKAJIMA, *Phys. Plasmas*, **3**, 4556 (1996).

6. C. NÜHRENBERG, *Phys. Plasmas*, **6**, 137 (1999).

7. J. CHEN, N. NAKAJIMA, and M. OKAMOTO, *Phys. Plasmas*, **6**, 1562 (1999).

8. W. A. COOPER, D. B. SINGLETON, and R. L. DEWAR, *Phys. Plasmas*, **3**, 275 (1996).

9. N. NAKAJIMA, S. R. HUDSON, C. C. HEGNA, and Y. NAKAMURA, *Nucl. Fusion*, **46**, 177 (2006).

10. C. C. HEGNA and N. NAKAJIMA, *Phys. Plasmas*, **5**, 1336 (1998).

11. S. R. HUDSON and C. C. HEGNA, *Phys. Plasmas*, **10**, 4716 (2003).